JACS
JOURNAL OF THE AMERICAN CHEMICAL SOCIETY
Article
pubs.acs.org/JACS

Wetting–Dewetting and Dispersion–Aggregation Transitions Are Distinct for Polymer Grafted Nanoparticles in Chemically Dissimilar Polymer Matrix

Tyler B. Martin,[†,§,#] Katrina Irene S. Mongcopa,[∥,#] Rana Ashkar,[⊗,○] Paul Butler,[⊗] Ramanan Krishnamoorti,[*,⊥] and Arthi Jayaraman[*,†,‡]

[†]Department of Chemical and Biomolecular Engineering, University of Delaware, Newark, Delaware 19716, United States
[‡]Department of Materials Science and Engineering, University of Delaware, Newark, Delaware 19716, United States
[§]Department of Chemical and Biomolecular Engineering, University of Colorado, Boulder, Colorado 80309, United States
[∥]Department of Materials Engineering, University of Houston, Houston, Texas 77004, United States
[⊥]Department of Chemical and Biomolecular Engineering, Department of Petroleum Engineering, Department of Chemistry, University of Houston, Houston, Texas 77004, United States
[⊗]National Institute of Standards and Technology Center for Neutron Research, Gaithersburg, Maryland 20899, United States
[○]Department of Materials Science and Engineering, University of Maryland, College Park, Maryland 20742, United States

Supporting Information

ABSTRACT: Simulations and experiments are conducted on mixtures containing polymer grafted nanoparticles in a chemically distinct polymer matrix, where the graft and matrix polymers exhibit attractive enthalpic interactions at low temperatures that become progressively repulsive as temperature is increased. Both coarse-grained molecular dynamics simulations, and X-ray scattering and neutron scattering experiments with deuterated polystyrene (dPS) grafted silica and poly(vinyl methyl ether) PVME matrix show that the sharp phase transition from (mixed) dispersed to (demixed) aggregated morphologies due to the increasingly repulsive effective interactions between the blend components is distinct from the continuous wetting–dewetting transition. Strikingly, this is unlike the extensively studied chemically identical graft–matrix composites, where the two transitions have been considered to be synonymous, and is also unlike the free (ungrafted) blends of the same graft and matrix homopolymers, where the wetting–dewetting is a sharp transition coinciding with the macrophase separation.

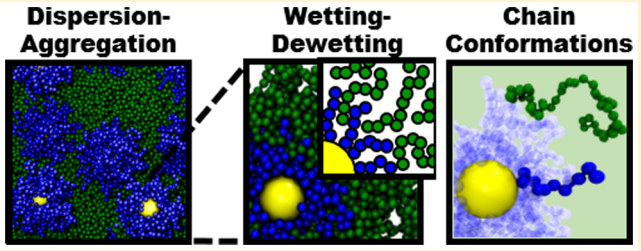

INTRODUCTION

Driven by the need to develop functionally superior materials, significant effort has been directed toward the understanding of structure and thermodynamics of polymer blends[1−5] and polymer–nanoparticle mixtures/blends.[6−11] Fundamentally, the delicate balance of enthalpic and entropic driving forces, arising from the interplay of polymer and particle chemistry, polymer molecular weight, architecture, particle size, and the blend composition, dictates the phase transition from mixed (dispersed) to demixed (aggregated) states. A large body of scientific work[10,12−22] has focused on the development of polymer nanocomposites wherein the particles are grafted with polymers in order to maximize the particle dispersibility in a chemically similar matrix polymer. Through these numerous studies that are described in review articles,[12,23−26] it is now well understood that the extent of matrix polymer penetration (exclusion) into the grafted polymer layer, also termed as "wetting" ("dewetting"), dictates extent of dispersion (aggregation) of polymer grafted particles in the free matrix polymer. Experiments, theory, and simulations have shown ways to tune this extent of wetting by varying the grafting density (mushroom to brush regimes), ratio of matrix to graft molecular weights, and particle size or curvature. Especially in the dense grafting regime, where the direct particle–particle interactions are screened,[27] the chemical similarity of the graft and matrix reduces the thermodynamic driving forces for wetting–dewetting to being purely entropic. While the gain in entropy of mixing drives wetting of the grafted polymer by the matrix chains, the conformational entropy loss due to matrix penetrating a dense grafted layer drives dewetting. Decreasing ratio of matrix to graft molecular weights,[24] increasing graft molecular weight dispersity,[27−31] and decreasing polymer flexibility[32] have been shown to increase the wetting and, in turn, stabilize particle dispersion.

Received: May 27, 2015
Published: August 3, 2015

DOI: 10.1021/jacs.5b05291
J. Am. Chem. Soc. 2015, 137, 10624−10631

While the wetting−dewetting and dispersion−aggregation phase behavior of *chemically identical* dense brush graft−matrix blends is largely governed by these entropic driving forces, there is a nontrivial competition between the enthalpic and entropic driving forces for *chemically dissimilar* graft−matrix composites. Theoretical studies of flat surfaces or colloids grafted with a dense polymer brush placed in a chemically dissimilar polymer matrix have predicted how the choice of chemically dissimilar graft and matrix polymers with negative or positive Flory−Huggins χ parameter (quantifying the enthalpic interactions between the blend components) impacts the graft conformations and the wetting−dewetting.[33−37] With the use of highly controlled synthesis and characterization techniques, a few experiments have also shown that particle dispersion and aggregation are tuned by enthalpic interactions between grafted and matrix chains.[37−40] Especially in the case where there are attractive enthalpic interactions between the graft and matrix chains, the mixture is driven to a dispersed phase even with grafts that are shorter than matrix chains, a case where chemically identical systems would exhibit dewetting and particle aggregation.[38] This ability to disperse particles due to graft−matrix miscibility allows for higher filler loadings than athermal chemically identical graft−matrix composites.[38] Choosing graft−matrix polymers with specific H-bonding also enables thermoreversibility to particle dispersion−aggregation.[40]

In the above studies, the wetting−dewetting transition and dispersion−aggregation transition have been assumed to occur simultaneously, and are treated synonymously.[10,12,20,22,24−26,41−44] In contrast, in this paper, using simulations and experiments, we show that in chemically dissimilar graft−matrix polymer nanocomposites, the wetting−dewetting transition occurs gradually with increasing temperature and is distinct from the sharp dispersion−aggregation (phase separation) transition. The coarse-grained molecular dynamics (CGMD) simulations focus on generic chemically dissimilar graft−matrix polymer pairs that exhibit a lower critical solution temperature (LCST) phase behavior with increasing temperature. The experiments focus on deuterated polystyrene (dPS) grafted silica particles in a poly(vinyl methyl ether) (PVME) matrix as dPS−PVME blends have been shown to exhibit miscibility at room temperature, and LCST phase behavior with increasing temperatures.[45] Through a comprehensive characterization of the composite using X-ray scattering and neutron scattering experiments, along with morphology and chain conformations from CGMD simulations, we provide the molecular mechanism underlying the gradual wetting to dewetting transition being separate from the sharp dispersion-to-aggregation transition.

METHODS

Simulations. Briefly, we represented the polymer grafted spherical nanoparticles in a polymer matrix using a generic coarse-grained model with the nanoparticles (denoted as P) represented as a rigid-body of several $D = 1d$ beads ($d \approx 1$ nm), and the graft (denoted as G) and matrix (denoted as M) polymers as bead−spring chains.[46,47] The nonbonded G−G and M−M interactions were modeled by a Lennard-Jones potential with $\varepsilon_{GG} = \varepsilon_{MM} = 0.5k_BT$. The nonbonded G−M interactions ε_{GM} were varied from $0.3k_BT$ to $0.8k_BT$; therefore, the reduced temperature defined as $T^* = 1/\varepsilon^*_{GM} = 1.25−3.33$. The P−P, P−G, and P-M interactions were modeled via a purely repulsive Weeks−Chandler−Andersen (WCA) potential with $\varepsilon = 1.0\ k_BT$.

In this paper, the filler fraction or blend composition was varied over $\phi_G = 0.13−0.20$, where ϕ_G is defined as

$$\phi_G = \frac{V_{grafts}}{V_{grafts} + V_{matrix}} \quad (1)$$

where V_X is the total volume occupied by component X in the simulation. These compositions were chosen as they were similar to the systems studied in the experiments. For all simulations, the total occupied volume fraction in the simulation box was maintained to be $\eta = 0.35$. We note that the total occupied volume fraction includes grafts, matrix, and particle beads. We maintained 60 000 matrix beads to enforce a *minimum* box size of $\approx 44d \times 44d \times 44d$, regardless of our chosen filler fraction. We conducted Brownian dynamics (BD) simulations in the canonical ensemble using the graphics processing unit based HOOMD-blue package.[48] At an integrator temperature of $T = 5.0$, the initial configuration was integrated using a Brownian Dynamics integrator for 5×10^6 time steps to both mix and relax the grafted and matrix chains. The simulation box was then compressed to the desired volume fraction over 1×10^7 steps, and then mixed again for 1.5×10^7 steps at the compressed state. We then varied the integrator temperature from $T = 5.0$ to $T = 1.0$ using 10, geometrically sized quenches over a period of 5×10^7 time steps. After the annealing was completed, we ran the simulations for an additional 5×10^7 time steps where we sampled the equilibrium configurations of the system every 5×10^5 time steps to calculate the ensemble averages of various thermodynamic and structural properties. All the details of our model, simulation method and analyses are in the Supporting Information (SI) computational methods section.

Experimental Preparation of Polymer-Grafted Nanoparticles. Initiator-functionalized silica nanoparticles (SiO_2−initiator) were prepared according to the procedure in ref 49 (see details in SI experimental methods section). Deuterated polystyrene-grafted SiO_2 nanoparticles (SiO_2−dPS) were then synthesized using a modified AGET ATRP reaction[50] where briefly, the Cu(II)Br catalyst and dNbpy ligand were combined with d-styrene in a flask and bubbled with nitrogen for 30 min. In another flask, the $Sn(EH)_2$ reducing agent and SiO_2−initiator were dissolved in toluene, purged with nitrogen and transferred to the first flask. The reaction mixture was then placed in an oil bath at 90 °C and allowed to proceed for ∼40 h. After polymerization, the reaction mixture was further diluted with tetrahydrofuran (THF), filtered through a column of neutral aluminum oxide to remove the catalyst, concentrated in vacuo and precipitated in excess amount of cold methanol. The recovered polymer-grafted nanoparticles were further purified through a mixed solvent precipitation method using toluene and methanol. This step ensured the removal of unfunctionalized silica nanoparticles as well as free ungrafted chains from the grafted hybrid sample (see SI experimental methods section). Prior to gel permeation chromatography (GPC) experiments to determine the polymer brush molecular weight, the grafted polymers were cleaved from the SiO_2 surface by first dissolving the hybrid nanoparticles in 2 mL of THF and then adding 2 mL of a 2% (v/v) solution of aqueous HF. After stirring the solution overnight, the polymer was precipitated in excess amount of methanol and dried under vacuum for at least 24 h. GPC measurements gave a brush molecular weight (M_w) of 33 000 g/mol and polydispersity index (M_w/M_n) of 1.27. The grafted nanoparticles (SiO_2−dPS33k) were also subjected to thermo-gravimetric analysis to calculate the polymer grafting density, determined to be ≈0.7 chain/nm^2.

Experimental Preparation of Nanocomposites. The nanocomposite was prepared following a simple solution mixing procedure. Initially, PVME (M_w = 226 000 g/mol, PVME226k) was dried at 70 °C under vacuum overnight and cooled down to room temperature prior to use. Afterwards, a 20:80 (by weight) blend composition of SiO_2−dPS33k/PVME226k was prepared by co-dissolving predetermined amounts of SiO_2−dPS33k and PVME226k in toluene and mixing at room temperature for at least 24 h. The polymer blend was obtained by precipitating the solution in a large excess of hexane and collecting the solid sample by vacuum filtration. The resulting composite was allowed to dry in air for 2 days and annealed at 60 °C under vacuum for at least 24 h before the scattering measurements were performed. The samples were heated from room temperature to

DOI: 10.1021/jacs.5b05291
J. Am. Chem. Soc. 2015, 137, 10624−10631

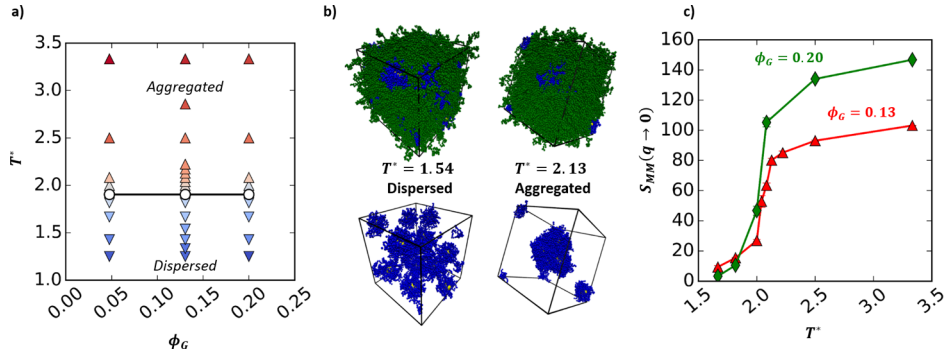

Figure 1. (a) Dispersion−aggregation phase-diagram; (b) simulation snapshots with bottom panel hiding the matrix polymer; and (c) low q-value of the matrix−matrix structure factor for particles of diameter $D = 5d$ grafted with "G" homopolymer chains of length $N_{graft} = 10$ and grafting density $\Sigma = 0.76$ chains/d^2 in a "M" homopolymer matrix of length $N_{matrix} = 50$ at a total volume fraction $\eta = 0.35$ and with blend composition $\phi_G = 0.13$ and 0.20. The total volume fraction, η, is defined as ratio of volume of all CG beads to the volume of the simulation box. The blend composition, ϕ_G, is defined as ratio of volume of graft CG beads to the volume of graft and matrix CG beads in the system. In part a, upward and downward triangles denote aggregated and dispersed states, respectively, in the simulations, and the circles denote the dispersion−aggregation transition. The snapshots in part b are for $\phi_G = 0.13$ blends. The error bars in part c are standard deviations calculated from 50 uncorrelated configurations for each system; the error bars when not visible are smaller than the size of the symbol.

elevated temperature for the scattering measurements. In some cases, the samples were also studied in cooling and we found reproducible data between heating and cooling as long as the temperature did not exceed 145 °C.

Additional details of the experimental methods can be found in the SI experimental methods section.

RESULTS AND DISCUSSION

Coarse-grained (CG) molecular dynamics (MD) simulations of homopolymer grafted particles in a chemically distinct homopolymer matrix were conducted for a blend with $N_{matrix} = 50$ Kuhn segments (or effective "monomers"), $N_{graft} = 10$ Kuhn segments, particle size $D = 5d$, where d is the size of the Kuhn segment, at grafting density of 0.76 chains/d^2 for two different blend/mixture compositions.

Figure 1a shows that there is a transition from particle dispersion to particle aggregation with increasing (reduced) temperature, T^*. The evidence of dispersion at this high matrix to graft molecular weight ratio is in contrast to the chemically similar graft−matrix blends, where aggregation is observed at high matrix to graft molecular weight purely due to entropic driving forces. The reason we see dispersion at low T^* for this high matrix to graft molecular weight ratio in this chemically dissimilar graft (G)−matrix (M) polymer pair system is because the attractive graft−matrix enthalpic interactions (negative χ) drive graft−matrix contacts at low T^*. This favorable enthalpic driving force for wetting or mixing overcomes the net entropic driving forces that favor graft−matrix dewetting or demixing, and result in well-dispersed blends. As the temperature is increased, the enthalpic forces become repulsive (positive χ) and along with the entropic driving forces favor demixing of grafted and matrix chains, and result in aggregated blends. The dispersion to aggregation transition is seen both in simulation snapshots rendered with the Visual Molecular Dynamics software (VMD)[51] (e.g., Figure 1b), as well as partial structure factors (MM, PP, and GG) (SI Figures S1−S3) which show an upturn with increasing temperature as $q \to 0$, indicative of the *onset of particle aggregation*. These partial structure factors are calculated via Fourier transform of MM, PP, and GG radial distribution functions, as described in the Supporting Information, and an upturn at low q indicates increasing aggregation of like-pairs, MM, PP, or GG. Since the simulations are run at discrete temperatures, the dispersion−aggregation phase transition (circles in Figure 1a) is marked as the temperature where we see the onset of the low-q upturn in these partial structure factors. The $S_{MM}(q \to 0)$ versus T^* data for the $\phi_G = 0.13$ and 0.20 compositions (Figure 1c) show a sharp transition over a small T^* range, indicating a first-order dispersion−aggregation transition. We are unable to resolve differences in the dispersion−aggregation T^* of $\phi_G = 0.13$ and 0.20 due to the discrete steps in T^* at which simulations are run.

Molecular simulations are also a powerful means to characterize the wetting to dewetting transition associated with the penetration of the grafted polymer chains by the chemically dissimilar matrix polymers. Using CGMD simulations, we calculated the extent of wetting in the dispersed and aggregated states using two different methods. In the first method, the graft and matrix Kuhn segment (or effective "monomer") concentration profiles (Figure 2a for $\phi_G = 0.13$, and SI Figure S4 for all ϕ_G) confirm that, with increasing temperature, there is a gradual decrease in overlap between graft and matrix monomer concentration profiles. In the second method, which results in a single number that characterizes the extent of wetting, we identify the spatial location of the anisotropic, closed isosurface corresponding to the edges of the aggregates (at high T^*) or isolated grafted particles (at low T^*), and then calculate the fraction of matrix monomers that are inside (wet) or outside (dewet) of this boundary as a function of temperature (Figure 2b). At any temperature, the magnitude of the wet monomer fraction increases with increasing amount of grafted polymer chains in the blends, as would be anticipated based on a simple volumetric scaling of the number of particles. On the other hand, when a normalized wet monomer fraction (normalized by the surface area of the aggregates) is calculated from these simulations, the data collapses onto a single curve irrespective of blend composition (not shown). Remarkably, we observe no discontinuous or abrupt change in the wetting shown in Figure 2 and instead observe a continuous transition.

Another important feature of the gradual wetting to dewetting transition (Figure 2) and the sharp dispersion to aggregation transition (Figure 1) is that the onset of dewetting occurs at a temperature well below the dispersion−aggregation

DOI: 10.1021/jacs.5b05291
J. Am. Chem. Soc. 2015, 137, 10624−10631

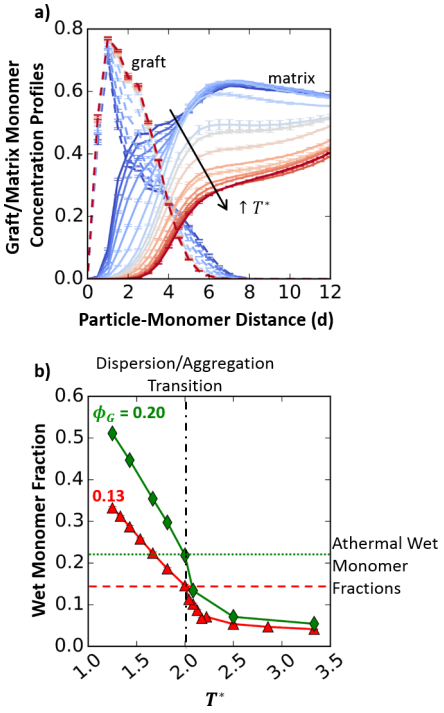

Figure 2. (a) Graft monomer (dashed lines) and matrix monomer (solid lines) concentration (in units of d^{-3}) versus distance from the particle surface at ϕ_G = 0.13. The graft concentration profile is calculated for each grafted particle independently and the average of these profiles is presented. In the calculation of each grafted particle's profile, we only include the contribution of grafts that are attached to the same particle, and do not include any inter-grafted particle contributions. (b) Wet monomer fraction versus reduced temperature, T^*. Also shown are the dispersion−aggregation transition temperature (vertical dot-dashed line) and the wet monomer fractions for the athermal ϕ_G = 0.13 and 0.20 blends (horizontal dashed and dotted lines). The error bars in parts a and b are standard deviations calculated from 50 uncorrelated configurations for each system; the error bars when not visible are smaller than the size of the symbol.

transition temperature, and that the dewetting continues at temperatures higher than the dispersion−aggregation transition. These observations imply that the wetting−dewetting and dispersion−aggregation are two *distinct* transitions. This is in contrast to past literature, especially for chemically similar graft−matrix systems, where the two transitions are treated *synonymously*.[10,12,20,22,24−26,41−44]

Interestingly, for a ϕ_G = 0.13 blend with all WCA excluded volume (athermal) interactions, that would mimic a chemically similar χ = 0 graft (G)−matrix (M) polymer pair with the same grafting density, particle size, matrix and graft chain lengths, the wet monomer fraction (horizontal dashed line in Figure 2b) coincides with the intersection of the wet-monomer fraction profile and dispersion−aggregation transition of the ϕ_G = 0.13 chemically dissimilar composite. This means that when the extent of wetting for the chemically dissimilar graft (G)−matrix (M) polymer system reaches the (threshold or critical) wetting seen in chemically similar athermal system, the chemically dissimilar graft−matrix system goes through the dispersion−aggregation transition.

We conducted Small Angle X-ray and Neutron scattering (SAXS and SANS) studies as a function of temperature on blends of 226k PVME (80 vol %) with 33k dPS-grafted silica particles (grafting density = 0.7 chains/nm^2). These scattering techniques provide structural information that covers a broad range of length scales, and can be compared to the simulation trends presented. Since the X-ray contrast between the polymers is small and their contrast with the silica particles dominate the SAXS data, we use this method and the observed peaks in the SAXS data to track the correlations between silica particles and therefore monitor the changes in wetting of the d-PS brushes on the silica particles. Separately, since the largest contrast for neutrons are between dPS and PVME (see SI experimental methods) and because of the small amount of silica particles in the scattering volume, we monitor the bulk phase behavior (and aggregation) of the dPS-grafted silica in PVME using the low q behavior in SANS.

It is well understood that sufficiently concentrated nanoparticles will exhibit a liquid like ordering characterized by a peak in the pair correlation function. This translates into a peak in the scattered intensity which is essentially the Fourier transform of the real space distribution of material. Thus, the first order peak in the scattered X-ray intensity, denoted q^* in Figure 3a, is a direct measure of the distance between silica particles and, in the case of no matrix or solvent, is a measure of the height of the brush as established by Goel et al.[52] The peak in the X-ray scattering from the blend of dPS grafted SiO_2 and PVME at room temperature in Figure 3a indicates the silica particles are fairly homogeneously dispersed. This is further confirmed through a direct space transmission electron micrograph shown in Figure 3e.

With increasing temperature, the primary scattering peak shifts to higher q indicating the silica particles are moving closer together. Since the concentration of particles does not change this is a clear indication of a depletion of the matrix polymers between particles, and thus strongly suggests that the PVME matrix chains are dewetting the dPS grafted layer. Parenthetically, we note that the dPS starts to dewet the portions of the grafted brush structure closest to the silica particle (and densest) first and progressively dewets portions farther away from the silica core with increasing temperature. Finally, at the highest temperature, the peak location almost coincides with that of the pure dPS-grafted SiO_2 nanoparticles in its melt state, indicating no matrix polymer is left between the nanoparticles, suggesting a complete dewetting and the formation of dense nanoparticle aggregates. The formation of nanoparticle aggregates is further confirmed by TEM of a sample held at 160 °C and is shown in Figure 3f. The peak position for the pure SiO_2−dPS33k nanoparticles (i.e., with no PVME added) gives the particle to particle distance in its space filling state, and thus the grafted brush height of ∼9 nm (SI Figure S5). The gradual shift of the peak position with temperature from evenly dispersed to "dry" grafted nanoparticle clusters suggests a gradual dewetting in agreement with the gradual decrease in wet monomer fraction seen in the simulations (Figure 2b).

The increase in low q intensity as a function of temperature in both the SAXS and SANS data indicates an increasing contribution of large-scale inhomogeneities. SAXS is only sensitive to silica density inhomogeneities within the polymer matrix, whereas the SANS data is sensitive to all three components, and in particular, the large neutron contrast between dPS and PVME make SANS especially sensitive to large-scale concentration fluctuations between dPS and PVME which would be characteristic of graft polymer−matrix polymer phase separation. We note that while the silica (especially as it aggregates) does contribute to the scattering in this q-regime, the magnitude of such scattering is small because of the small

DOI: 10.1021/jacs.5b05291
J. Am. Chem. Soc. 2015, 137, 10624−10631

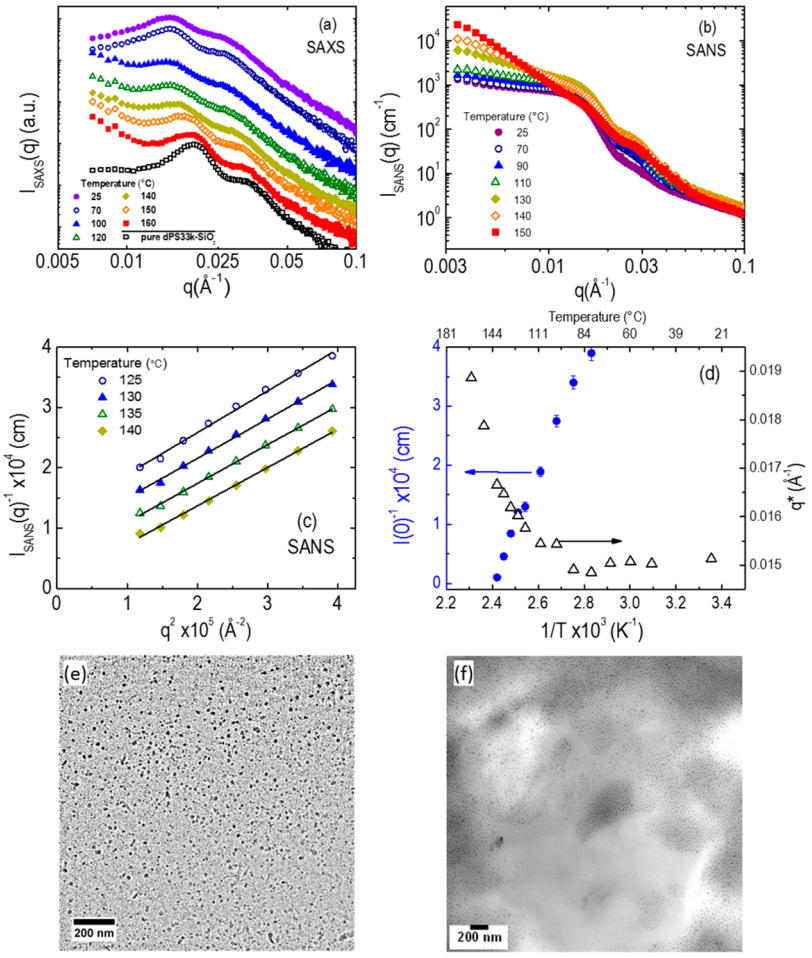

Figure 3. (a) Temperature dependence of Small Angle X-ray Scattering (SAXS) intensity data for blends of a 33k dPS-grafted silica (grafting density of 0.7 chains/nm^2) with a 226k PVME at a blend composition of 80% PVME by volume; data for the scattering intensity from a pure 33k dPS-grafted silica particles with no PVME matrix are shown for comparison. (b) Temperature dependence of the Small Angle Neutron Scattering (SANS) intensity for the blend described in (a). (c) Ornstein–Zernike representation of selected SANS data to estimate the intensity in the forward angle ($I(0)$) and correlation length (ξ) as a function of temperature for the single phase blends. (d) Temperature dependence of $I^{-1}(0)$ from SANS and primary scattering peak position (q^*) from SAXS for the blend described in (a) and (b). TEM images of thin sections of unstained blends at (e) 25 °C showing individually dispersed nanoparticles and after annealing at (f) 160 °C showing large-scale phase separation.

volume fraction of silica used in these samples and therefore we adopt a pseudobinary approach to analyze the SANS data. Indeed, the increase in the low q SANS intensity data (Figure 3b) is consistent with a lower critical solution temperature (LCST) system where the concentration fluctuations increase with increasing temperature. For a binary blend, the scattering at low q in such a system can be described by the Ornstein-Zernike equation:

$$I_{\mathrm{SANS,Coh}}(q) = \frac{I(0)}{1 + \xi^2 q^2} \tag{2}$$

where ξ is the correlation length. The scattered intensity in the forward direction, $I(0)$, is obtained by extrapolating the $1/I(q)$ vs q^2 data to $q = 0$ (Figure 3c). Both the zero-angle scattering intensity, $I(0)$, and correlation length ξ diverge as the spinodal temperature is approached (SI Figure S6). Plotting $1/I(0)$ and $1/\xi^2$ against $1/T$ (Figure 3c and Figure S6) allows a linear extrapolation to $q = 0$, and leads to the identification of the spinodal temperature, $T_s \sim 143 \pm 2$ °C. The behavior of the intensity and correlation length with temperature bears remarkable similarity to that observed for polymer blends and star-PS/PVME mixtures.[53,54]

These dPS (graft)–PVME (matrix) blend experiments are thus in remarkable agreement with the simulations using a generic LCST graft–matrix pair, suggesting that (a) the wetting to dewetting transition is a gradual process with increasing temperature while the dispersion–aggregation or macrophase separation transition is first order, (b) the onset of wetting to dewetting occurs at temperatures *lower than* the dispersion to aggregation transition, and (c) dewetting continues at temperatures above the spinodal temperature in the aggregated state.

To better understand the chain conformations that are linked to the above wetting–dewetting behavior, we unravel the effect of grafting one of the polymers in the LCST graft (G)–matrix (M) polymer pair, on the enthalpic and entropic driving forces of the phase behavior. To do this we also simulate using CGMD a blend of ungrafted (G) polymer and ungrafted (M) polymer, termed the *free blend,* with the same number of G and M chains and chain lengths as the *grafted* blend, for the blend compositions discussed so far. Figure 4a shows that, for the free blend, the transition from mixed to demixed states occurs at higher temperatures and has a stronger dependence on the blend composition than the grafted blend. We explain this difference between the free and grafted blends through the

DOI: 10.1021/jacs.5b05291
J. Am. Chem. Soc. 2015, 137, 10624–10631

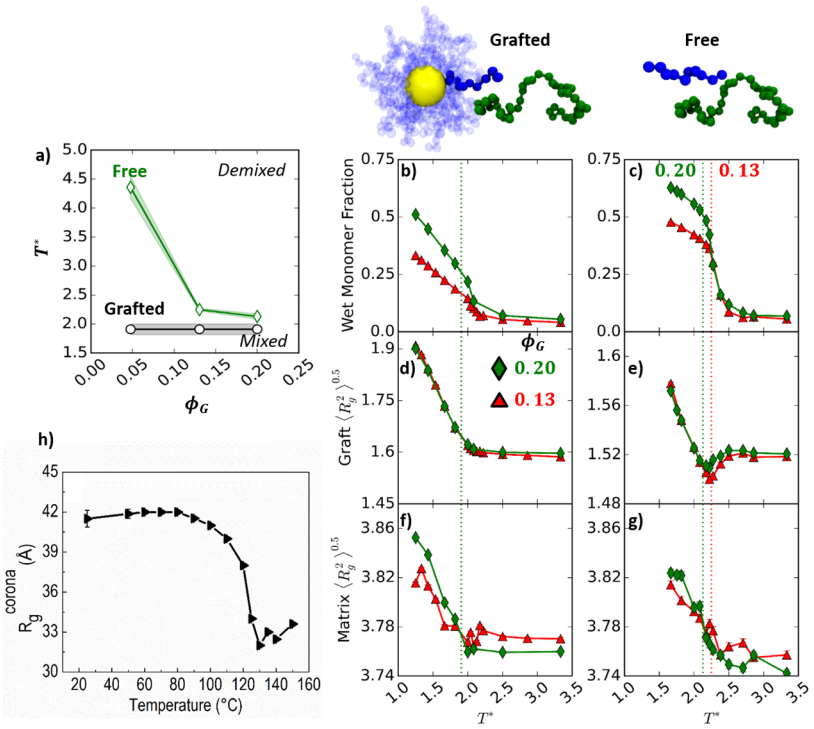

Figure 4. (a) Mixed−demixed phase-diagram comparing the grafted or free blend, the wet monomer fraction vs temperature (b and c), graft radius of gyration (d and e), and matrix radius of gyration (f and g) for particles of diameter $D = 5d$ grafted with chains of length $N_{graft} = 10$ and grafting density $\Sigma = 0.76$ chains/d^2 in a matrix of length $N_{matrix} = 50$ (a, b, d, and f) or blends of $N_{graft} = 10$ and $N_{matrix} = 50$ chains (a, c, e, and g) at a total volume fraction $\eta = 0.35$ and filler fractions $\phi_G = 0.13$ (triangles), and 0.20 (diamonds). The error bars in parts b−g are standard errors calculated from 50 uncorrelated configurations for each system; the error bars when not visible are smaller than the size of the symbol. (h) Change in experimentally measured radius of gyration of the outer shell (called R_g^{corona}) with temperature from an excluded volume model for blends of a 33k dPS-grafted silica (grafting density of 0.7 chains/nm^2) with a 226k PVME at a blend composition of 80% PVME by volume. We note that R_g^{corona} does not represent the overall dimension of the polymer chains but only the outer shell of the grafted chains.

enthalpic and entropic contributions to the change in free energy to go from mixed (dispersed) to demixed (aggregated) states, ΔA, defined as

$$\Delta A_{\text{mixed}\rightarrow\text{demixed}} = \Delta U - T\Delta S \quad (3)$$

where ΔU is the change in internal energy and ΔS the change in entropy going from mixed (dispersed) to demixed (aggregated) states.

If we assume that the G−M attractive interactions are the dominant energetic driving force for G−M mixing, we can define $\Delta U \sim \Delta n \varepsilon_{GM}$, where Δn is the change in number of contacts between G and M monomers going from mixed (dispersed) to demixed (aggregated) states, and ε_{GM} the attractive interaction strength between G and M monomers. Since both free and grafted blends have the same number of G and M monomers, the total number of *possible* G−M monomer contacts should be the same for the grafted and free blends. However, in the grafted blend, the dense grafting shields some of the G monomers from making contacts with the M monomers in the mixed (dispersed) state, as seen in the monomer concentration profiles in Figure 2a. It is fair to assume that in the demixed (aggregated) state, the number of G−M contacts is minimal and negligibly different between the grafted and free blend. Thus, the (negative) Δn and (positive) ΔU going from mixed (dispersed) to demixed (aggregated) states is smaller for the grafted blend than the free blend.

The major contributions to the change in entropy going from mixed (dispersed) to demixed (aggregated) states is the conformational entropy gain of matrix chains, ΔS_{conf}, and mixing entropy loss, ΔS_{mix}. Even though these two contributions to entropy cannot be fully decoupled, it is useful to see individually how these impact the total entropy change.

ΔS_{conf}, the conformational entropy gain of the matrix chains going from mixed (dispersed) to demixed (aggregated) state, is larger for the grafted blend than the free blend. This is because the M matrix chains that penetrate the grafted layer in the dispersed state have fewer conformations in the crowded grafted G layer than they do outside the grafted layer in the aggregated state. In contrast, we expect that the free blend has relatively negligible differences in matrix conformations in the mixed and demixed state. ΔS_{mix}, the mixing entropy loss going from mixed (dispersed) to demixed (aggregated) state, is smaller for the grafted blend than for the free blend.[55] This is because in the mixed state, due to the G chains being end-grafted to the particle surface in the grafted case, the volume available for G and M monomer mixing is significantly lower in the grafted blends compared to the free blends. In the demixed state, the grafted and free blends should have similar low mixing entropy.

Thus, with a larger energetic and entropic driving force to stay mixed, the free blends have a higher mixed-to-demixed transition temperature than the grafted blends. The grafted vs free blend phase behavior is, thus, not surprising due to the above intuitive thermodynamic driving forces.

Surprisingly, in contrast to the gradual continuous transition of wet monomer fraction with increasing temperature for the grafted blends, for free blends, the wet monomer fractions, which characterize the extent of G−M monomer mixing, show

DOI: 10.1021/jacs.5b05291
J. Am. Chem. Soc. 2015, 137, 10624−10631

a sharp transition with increasing temperature. Furthermore, for the ϕ_G = 0.13 and 0.20 free blends, this mixing−demixing transition coincides with the macrophase separation transition (dotted lines), in contrast to the grafted blends at those compositions. We conjecture that the gradual wetting to dewetting transition for the grafted blend/composite in contrast to the sharp transition for the free blend is due to the permanent tethering of the grafted chains. Tethering of graft chains to the particle creates regions in the grafted layer with variable entropic driving forces for graft−matrix mixing. With increasing distance from the particle surface, each successive layer of grafted monomers has increased free volume available for mixing with matrix monomers. This creates a gradient in graft−matrix mixing entropy gain and conformational entropy loss upon wetting. For example, the grafted region closest to the particle center has a higher conformational entropy loss and lower mixing entropy gain from graft−matrix wetting than the outer region in the grafted layer. Thus, as the temperature increases likely various regions of the grafted layers are dewet in a step by step fashion rather than sharply as in the case of free blends. While curvature of the grafted surface affects the available volume for mixing within the grafted layer, the gradual wetting to dewetting transition is also seen in zero-curvature flat surface limit (SI Figure S8). This further strengthens the argument that the grafting/tethering of one of the polymers in the blend leads to the gradual continuous wetting to dewetting transition.

To elucidate the single chain conformations within the blends during this sharp vs continuous wetting−dewetting phenomena for free blends vs grafted blends, respectively, we calculate the ensemble average radius of gyration for the G and M chains in the grafted and free blends. There are clear differences between the behavior of the G homopolymer chains when grafted (Figure 4d) and free (Figure 4e). First, due to dense grafting-induced chain extension, the size of the G chains in the grafted systems is larger than those in the free blends. Second, as temperature increases, coinciding with the wetting−dewetting transition, the grafted G chains' sizes decrease gradually until they plateau to a value when the system has completed the wetting to dewetting transition. In contrast, the free G polymer chains go through a coil−globule−coil transition, coinciding with the mixing-demixing transition in the free blend. In this case it has been argued that as the temperature increases, the (minority component) G chains have an increasing drive to shrink or collapse to a globule because they are amidst increasingly unfavorable M matrix chains. Once macrophase separation occurs, the G chains are in a domain of other G chains and are able to relax their entropically unfavorable globule configurations and expand modestly. In the grafted blend, the segregation of the G chains in the grafted layer decreases the need for the G chains to collapse to the same extent as free G chains, as the grafted architecture prevents single G chains from ever being totally surrounded by M chains. Additionally, the dense grafting also prevents the G chains from going through the drastic changes in chain conformations that they do in the free blends. Interestingly, applying an excluded volume model[56] to quantitatively model the SANS data for the dPS-grafted SiO_2 and PVME blends, allows for the extraction of a radius of gyration of the outer layer of the grafted chains (Figure 4h). The decreasing radius of gyration of the outer layer of the grafted chains in experiments (Figure 4h) and decreasing graft radius of gyration in molecular simulations (Figure 4d) are remarkably similar. The matrix M chains in the grafted and free blends adopt similar chain conformations at all ϕ_G, with the effect of temperature on the matrix chain conformations decreasing with decreasing ϕ_G for both free and grafted blends.

In summary, through a combination of coarse-grained simulations and X-ray and neutron scattering, we demonstrate that, unlike chemically identical graft−matrix systems, the sharp dispersion to aggregation transition is distinct from the gradual continuous wetting to dewetting transition in a polymer nanocomposite with a chemically dissimilar graft−matrix polymer pair that exhibits LCST behavior. We also show that the dispersion to aggregation transition occurs when the extent of wetting in the attractive graft−matrix polymer composite approaches that of the analogous chemically similar graft−matrix polymer composite.

■ ASSOCIATED CONTENT

Supporting Information

The Supporting Information is available free of charge on the ACS Publications website at DOI: 10.1021/jacs.5b05291.

Detailed computational and experimental methods, data supporting the discussion in the main article (PDF)

■ AUTHOR INFORMATION

Corresponding Authors

*arthij@udel.edu

*ramanan@uh.edu

Author Contributions

#T.B.M. and K.I.S.M.: equal contributions.

Notes

The authors declare no competing financial interest.

■ ACKNOWLEDGMENTS

A.J. acknowledges financial support from U.S. Department of Energy under Grant DE-SC0003912 and T.B.M. acknowledges financial support from NSF graduate fellowship (award number DGE 1144083). R.K. and K.I.S.M. acknowledge financial support from ExxonMobil Chemical Company. We acknowledge B. Natarajan for assistance with the TEM images. SAXS data were obtained using an instrument obtained on a National Science Foundation (NSF DMR 1040446) funded instrument. This work used NERSC supercomputing supported by the U.S. Department of Energy (DE-AC02- 05CH11231), the Farber supercomputer at University of Delaware, and the Opuntia supercomputer at University of Houston. This work utilized the NIST Center for Neutron Research (NCNR) supported in part by the National Science Foundation under Grant No. DMR-0944772.

■ REFERENCES

(1) McMaster, L. P. *Macromolecules* **1973**, *6*, 760.

(2) Bates, F. S. *Science* **1991**, *251*, 898.

(3) Paul, D. R.; Bucknall, C. B. *Polymer Blends: Formulation and Performance (Two volume set)*; Wiley: New York, 2000.

(4) Ryan, A. J. *Nat. Mater.* **2002**, *1*, 8.

(5) Eitouni, H.; Balsara, N. In *Physical Properties of Polymers Handbook*; Mark, J., Ed.; Springer: New York, 2007; p 339.

(6) Mackay, M. E.; Tuteja, A.; Duxbury, P. M.; Hawker, C. J.; Van Horn, B.; Guan, Z.; Chen, G.; Krishnan, R. S. *Science* **2006**, *311*, 1740.

(7) Balazs, A. C.; Emrick, T.; Russell, T. P. *Science* **2006**, *314*, 1107.

(8) McGarrity, E. S.; Frischknecht, A. L.; Frink, L. J. D.; Mackay, M. E. *Phys. Rev. Lett.* **2007**, *99*, 238302.

DOI: 10.1021/jacs.5b05291
J. Am. Chem. Soc. 2015, 137, 10624−10631

(9) Sen, S.; Xie, Y. P.; Kumar, S. K.; Yang, H. C.; Bansal, A.; Ho, D. L.; Hall, L.; Hooper, J. B.; Schweizer, K. S. *Phys. Rev. Lett.* **2007**, *98*, 128302.
(10) Akcora, P.; Liu, H.; Kumar, S. K.; Moll, J.; Li, Y.; Benicewicz, B. C.; Schadler, L. S.; Acehan, D.; Panagiotopoulos, A. Z.; Pryamitsyn, V.; Ganesan, V.; Ilavsky, J.; Thiyagarajan, P.; Colby, R. H.; Douglas, J. F. *Nat. Mater.* **2009**, *8*, 354.
(11) Crawford, M. K.; Smalley, R. J.; Cohen, G.; Hogan, B.; Wood, B.; Kumar, S. K.; Melnichenko, Y. B.; He, L.; Guise, W.; Hammouda, B. *Phys. Rev. Lett.* **2013**, *110*, 196001.
(12) Green, P. F. *Soft Matter* **2011**, *7*, 7914.
(13) Corbierre, M. K.; Cameron, N. S.; Sutton, M.; Laaziri, K.; Lennox, R. B. *Langmuir* **2005**, *21*, 6063.
(14) Goel, V.; Chatterjee, T.; Bombalski, L.; Yurekli, K.; Matyjaszewski, K.; Krishnamoorti, R. *J. Polym. Sci., Part B: Polym. Phys.* **2006**, *44*, 2014.
(15) Tsubokawa, N. *Polym. J.* **2007**, *39*, 983.
(16) Kim, B. J.; Bang, J.; Hawker, C. J.; Kramer, E. J. *Macromolecules* **2006**, *39*, 4108.
(17) Lan, Q.; Francis, L. F.; Bates, F. S. *J. Polym. Sci., Part B: Polym. Phys.* **2007**, *45*, 2284.
(18) Shull, K. R. *J. Chem. Phys.* **1991**, *94*, 5723.
(19) Harton, S. E.; Kumar, S. K. *J. Polym. Sci., Part B: Polym. Phys.* **2008**, *46*, 351.
(20) Trombly, D. M.; Ganesan, V. *J. Chem. Phys.* **2010**, *133*, 154904.
(21) Xu, C.; Ohno, K.; Ladmiral, V.; Composto, R. J. *Polymer* **2008**, *49*, 3568.
(22) Jayaraman, A. *J. Polym. Sci., Part B: Polym. Phys.* **2013**, *51*, 524.
(23) Krishnamoorti, R.; Vaia, R. A. *J. Polym. Sci., Part B: Polym. Phys.* **2007**, *45*, 3252.
(24) Kumar, S. K.; Jouault, N.; Benicewicz, B.; Neely, T. *Macromolecules* **2013**, *46*, 3199.
(25) Chevigny, C.; Dalmas, F.; Di Cola, E.; Gigmes, D.; Bertin, D.; Boue, F.; Jestin, J. *Macromolecules* **2011**, *44*, 122.
(26) Ganesan, V.; Jayaraman, A. *Soft Matter* **2014**, *10*, 13.
(27) Martin, T. B.; Jayaraman, A. *Macromolecules* **2013**, *46*, 9144.
(28) Nair, N.; Wentzel, N.; Jayaraman, A. *J. Chem. Phys.* **2011**, *134*, 194906.
(29) Rungta, A.; Natarajan, B.; Neely, T.; Dukes, D.; Schadler, L. S.; Benicewicz, B. C. *Macromolecules* **2012**, *45*, 9303.
(30) Martin, T. B.; Dodd, P. M.; Jayaraman, A. *Phys. Rev. Lett.* **2013**, *110*, 018301.
(31) Natarajan, B.; Neely, T.; Rungta, A.; Benicewicz, B. C.; Schadler, L. S. *Macromolecules* **2013**, *46*, 4909.
(32) Lin, B.; Martin, T. B.; Jayaraman, A. *ACS Macro Lett.* **2014**, *3*, 628.
(33) Borukhov, I.; Leibler, L. *Macromolecules* **2002**, *35*, 5171.
(34) Borukhov, I.; Leibler, L. *Phys. Rev. E: Stat. Phys., Plasmas, Fluids, Relat. Interdiscip. Top.* **2000**, *62*, R41.
(35) Laub, C. F.; Koberstein, J. T. *Macromolecules* **1994**, *27*, 5016.
(36) Muller, M.; MacDowell, L. G. *Europhys. Lett.* **2001**, *55*, 221.
(37) Kim, B.; Ryu, D. Y.; Pryamitsyn, V.; Ganesan, V. *Macromolecules* **2009**, *42*, 7919.
(38) Ojha, S.; Dang, A.; Hui, C. M.; Mahoney, C.; Matyjaszewski, K.; Bockstaller, M. R. *Langmuir* **2013**, *29*, 8989.
(39) Brown, H. R.; Char, K.; Deline, V. R. *Macromolecules* **1990**, *23*, 3383.
(40) Heo, K.; Miesch, C.; Emrick, T.; Hayward, R. C. *Nano Lett.* **2013**, *13*, 5297.
(41) Kalb, J.; Dukes, D.; Kumar, S. K.; Hoy, R. S.; Grest, G. S. *Soft Matter* **2011**, *7*, 1418.
(42) Jiao, Y.; Akcora, P. *Macromolecules* **2012**, *45*, 3463.
(43) Sunday, D.; Ilavsky, J.; Green, D. L. *Macromolecules* **2012**, *45*, 4007.
(44) Martin, T. B.; Jayaraman, A. *Soft Matter* **2013**, *9*, 6876.
(45) Nishi, T.; Wang, T. T.; Kwei, T. K. *Macromolecules* **1975**, *8*, 227.
(46) Ceperley, D.; Kalos, M. H.; Lebowitz, J. L. *Phys. Rev. Lett.* **1978**, *41*, 313.
(47) Grest, G. S.; Kremer, K. *Phys. Rev. A: At., Mol., Opt. Phys.* **1986**, *33*, 3628.
(48) HOOMD-blue Home Page. http://codeblue.umich.edu/hoomd-blue/.
(49) Pyun, J.; Jia, S.; Kowalewski, T.; Patterson, G. D.; Matyjaszewski, K. *Macromolecules* **2003**, *36*, 5094.
(50) Jakubowski, W.; Matyjaszewski, K. *Macromolecules* **2005**, *38*, 4139.
(51) Humphrey, W.; Dalke, A.; Schulten, K. *J. Mol. Graphics* **1996**, *14*, 33.
(52) Goel, V.; Pietrasik, J.; Dong, H. C.; Sharma, J.; Matyjaszewski, K.; Krishnamoorti, R. *Macromolecules* **2011**, *44*, 8129.
(53) Faust, A. B.; Sremcich, P. S.; Gilmer, J. W.; Mays, J. W. *Macromolecules* **1989**, *22*, 1250.
(54) Russell, T. P.; Fetters, L. J.; Clark, J. C.; Bauer, B. J.; Han, C. C. *Macromolecules* **1990**, *23*, 654.
(55) Daoud, M. *Macromolecules* **1991**, *24*, 6748.
(56) Hammouda, B. In *Polymer Characteristics*; Springer: Berlin, Heidelberg, 1993; Vol. *106*, p 87.

DOI: 10.1021/jacs.5b05291
J. Am. Chem. Soc. 2015, 137, 10624−10631